A PLANAR QUASI-STATIC CONSTRAINT MODE TIRE MODEL

Rui Ma[a]
John B. Ferris[a]
Alexander A. Reid[b]
David Gorsich[b]

[a] Vehicle Terrain Performance Laboratory, Virginia Tech Mechanical Engineering Department

[b] US Army Tank Automotive Research, Development and Engineering Center (TARDEC)

ABSTRACT

The world of vehicle design is a fast-paced iterative environment that demands efficiency in the simulation of suspension loads. Toward that end, a computationally efficient, linear, planar, quasi-static tire model is developed in this work that accurately predicts a tire's lower-frequency, reasonably large amplitude, nonlinear stiffness relationship. Hamilton's principle is used to derive the axisymmetric and circumferentially isotropic stiffness equation which is discretized into segments to create the tire stiffness model. The model is parameterized by a single stiffness parameter and two shape parameters such that the tire's deformed shape is completely independent of the overall tire stiffness and the forces acting on the tire. Constraint modes are developed that capture the tire enveloping and bridging properties via component mode synthesis originated by Hurty and Gladwell and the Guyan static reduction method decouples active constraints from the stiffness matrix formulation. A recursive method is developed to deduce the set of active constraints at the tire-road interface. The model captures the nonlinear stiffness of a real tire by enforcing the unidirectional geometric boundary conditions during the recursive method. The model parameters are identified via two quasi-static experiments: a flat-plate and a cleat test. The simulated vertical loads are within 4% of the experimental load throughout a reasonably large range of travel for the flat-plate test and within 7% of the experimental loads for the cleat test. The simulation produces nonlinear stiffness when simulating a flat plate test and a discontinuous stiffness when simulating a cleat test. This model strikes a balance between simple tire models that lack the fidelity to make accurate chassis load predictions and computationally intensive models that cannot provide timely predictions. It is expected that this tire model is used as an integral part of computationally efficient and accurate vehicle simulations that are critical throughout the fast-paced iterative design process.

Keywords: Terrain Surface, Road Surface, Tire Force Estimation, Planar Tire Model, Constraint Mode

DISCLAIMER

NOMENCLATURE

N Total number of tire segments

$\boldsymbol{u}$ Set of radial deflections

R Tire radius

F_n Radial force acting on n^{th} tire segment

$\boldsymbol{F}^a$ Set of active radial tire force

Report Documentation Page

Form Approved
OMB No. 0704-0188

1. REPORT DATE	2. REPORT TYPE	3. DATES COVERED
10 JUL 2015		**00-00-2015 to 00-00-2015**

4. TITLE AND SUBTITLE	5a. CONTRACT NUMBER
A Planar Quasi-Static Constraint Mode Tire Model	5b. GRANT NUMBER
	5c. PROGRAM ELEMENT NUMBER
6. AUTHOR(S)	5d. PROJECT NUMBER
Rui Ma; John Ferris; Alexander Reid; David Gorsich	5e. TASK NUMBER
	5f. WORK UNIT NUMBER
7. PERFORMING ORGANIZATION NAME(S) AND ADDRESS(ES) **US Army RDECOM-TARDEC,6501 E. 11 Mile Road,Warren,MI,48397-5000**	8. PERFORMING ORGANIZATION REPORT NUMBER
9. SPONSORING/MONITORING AGENCY NAME(S) AND ADDRESS(ES)	10. SPONSOR/MONITOR'S ACRONYM(S)
	11. SPONSOR/MONITOR'S REPORT NUMBER(S)

12. DISTRIBUTION/AVAILABILITY STATEMENT
Approved for public release; distribution unlimited

13. SUPPLEMENTARY NOTES

14. ABSTRACT
See Report

15. SUBJECT TERMS

16. SECURITY CLASSIFICATION OF:			17. LIMITATION OF ABSTRACT	18. NUMBER OF PAGES	19a. NAME OF RESPONSIBLE PERSON
a. REPORT **unclassified**	b. ABSTRACT **unclassified**	c. THIS PAGE **unclassified**	**Same as Report (SAR)**	**12**	

F Vertical spindle force

f Linearly distributed load density

κ Radial stiffness density

E Elastic modulus

I Second moment of inertia

G Shear modulus

A Cross-sectional area

U_b Distributed bending potential energy

U_s Distributed shear potential energy

U_r Distributed radial elastic potential energy

U_w Distributed external work

γ_b Distributed bending stiffness

γ_s Distributed shear stiffness

γ_r Distributed radial stiffness

k_0 Model stiffness parameter

α_1, α_2 Model shape parameters

INTRODUCTION

With the advent of autonomous vehicles and the simultaneous pressure to improve energy efficiency, there are ever increasing demands on vehicle engineers. In particular, chassis engineers are faced with numerous design challenges (weight, cost, ride, handling, noise, reliability, packaging…) while interacting with several influential groups (scientific labs, proving ground, suppliers, safety, manufacturing, powertrain, body…) that result in a highly iterative design process. All these challenges and groups must be satisfied, to the best of the engineer's ability, within a very short timeframe. This fast-paced iterative design environment demands efficiency. Yet some fundamental physical truths remain within this cacophony of ever-changing requirements, influential groups, and deadlines. For example, regardless of how the power is developed, or how the wheels are steered, all the vehicle forces must ultimately be reacted through the vehicle suspension and tires.

The goal then, is to create a highly efficient model that captures the fundamental physical properties of tires from which simulation results are used to make informed design decisions. High fidelity, but computationally intensive models that provide very accurate information after the parts have been released for production are of no use. Simulation results arising from overly simplified models that lack the fidelity to make accurate chassis load predictions cannot be trusted and have little value. The objective of this work is to develop a computationally efficient, planar tire model that accurately predicts the lower-frequency, but not necessarily low amplitude, tire shape. Higher-frequency dynamics such as those that would be required for noise predictions are outside the scope of this work. The emphasis is intentionally placed on the shape of the deformed tire in the region of the contact patch, which must be capable of representing the bridging property (over narrow cracks) and enveloping property (over sharp bumps). The scope includes relatively large deformations, approaching, but not including, the point of rim strike. Although the relationship between the radial deformation and radial load is developed as a linear quasi-static model, the nonlinear stiffness relationship between the vertical spindle load and the vertical tire deflection that exists in real tires is captured by the model via the unidirectional geometric boundary condition at the tire-road interface. Six physical tire properties (radius, bending stiffness…) are reduced in the development of this model to a single stiffness parameter and two shape parameters. Experimental data are used to validate the approach using two quasi-static tests, a flat plate and a cleat test, with relatively large deformations.

The remainder of this work is developed as follows. Some background on finite element and finite difference tire modeling and the use of constraint modes in tire modeling is briefly reviewed. The mathematical derivation of the

parameterization of the stiffness matrix is developed followed by the development of the constraint mode model for this work. A recursive process to determine the proper tire shape is developed followed by validation with quasi-static experimental results. The resulting model is capable of bridging and enveloping irregularities in the road surface, generating the correct tire shape over irregular surfaces, and capturing the nonlinear stiffness relationship produced by physical tires.

BACKGROUND

One long-standing hurdle to accurately predicting responses (forces, torques, and accelerations) at the tire spindle is the development of high fidelity tire models. A considerable amount of tire modeling research has been conducted and a comprehensive review of the current state of the art is presented by Willumeit and Boehm [1] and more recently by Umsrithong [2]. Although a complete review of recent developments is not presented herein, the results from several of these works have direct relevance to the objectives of this study.

Researchers using Finite Element (FE) models have demonstrated that spindle responses can be predicted accurately, but may be computationally intensive and require a great number of physical parameters that are difficult or costly to obtain. Mousseau and Hulbert [3] and Darnell, Hulbert, and Mousseau [4] developed a 3-D tire model using an FE model for the tread and a lookup table for the sidewall membrane elements. Hanley, Crolla, and Hauke [5], used a 1-D FE model for tires traversing large obstacles; a more computationally efficient means to simulate relatively large deflections is pursued in the present study. Burke and Olatunbosun [6] used an FE model and a contact patch description to predict vertical force and displacement. Presently a more formal approach to defining the contact patch is developed through the definition of the active constraints between the tire and road surfaces. The current state of FE modeling work is presented by Ragheb, El-Gindy, and Kishawy [7] wherein Mooney-Rivlin material properties were used to create detailed FE models of the tread and tire. Their quasi-static flat-plate test results are used as a baseline to validate the capability of the work developed in the present study.

Other researchers have developed ring models of tires using finite differences. Van Oosten and Jansen [8] used a rigid ring to calculate belt vibrations while the deformed shape of the tire (including bridging and enveloping) was accurately predicted by Zegelaar and Pacejka by using a flexible ring to simulate the quasi-static response of a tire rolling over an uneven surface [9]. Although the simulation results agreed with the experimental data, the model is computationally intensive and requires comprehensive physical testing to define the parameters. A similar approach was developed by Loo, who modeled the tire by using a more complex flexible circular ring under tension with a nest of linear springs and dampers arranged radially [10]. However in Loo's study the ring tension and foundation stiffness requires additional contact patch measurements and the parameters were experimentally identified using multiple single-point load tests. Badalamenti et al. showed that a radial spring tire model, in which the radial spring element deflection depends on the adjacent element deflections, could accurately describe the tire enveloping behavior in an efficient model [11]. Presently, a planar ring model with an elastic foundation that includes shear and bending stiffness in ring is developed to accurately and efficiently describe the tire enveloping behavior.

It is assumed in this work that the low-frequency deformation of the tire shape can be adequately defined by the quasi-static constraint modes. This assumption is given credence by Gillespie's study in which a radial spring model is used to simulate the stiffness variation circumferentially and the magnitude of the radial force variation is found to be relatively independent of speed [12]. Similarly, Takayama et al. developed a model to predict the transient response of a tire encountering a cleat, where the belt and tread region is modeled by a rigid ring and deflections from the cleat are absorbed by a linear and planar spring attached to the rigid ring [13].

Ferris suggests that a static constraint mode tire model can be used to capture the tire enveloping and bridging properties with an axisymmetric and circumferentially isotropic model [14]. This reduced representation of the tire model is founded on the seminal component mode synthesis work originated by Hurty [15] and Gladwell [16]. Presently, in Equations (15)-(18), the order of the stiffness matrix is reduced via a Guyan static reduction [17]. This constraint mode tire model was expanded by Ma to include shear effects in the derivation and to reduce the required number of parameters from five dependent parameters to two parameters that define the constraint modes (the shape) and an independent parameter that defines the overall tire stiffness [18]. Presently, these concepts are combined to develop a complete formulation of the planar constraint mode tire model.

MODEL DEVELOPMENT

Consider the tire to be a ring that is inextensible in total circumference, but radially flexible, and supported by an elastic foundation parameterized by the radial stiffness, κ, as shown in Figure 1a. The assumed axisymmetric, planar, and circumferentially isotropic tire is divided into N segments. Each segment is modeled as an Euler elastic beam of length $2\pi R/N$ and notional cross-sectional area, A, shown as a shaded region in Figure 1b (the model itself is planar). The vector $\{\boldsymbol{u}\}$ defines the radial deflection of all tire segments and the quasi-static constraint modes are developed from the stiffness relationship given in Equation (1).

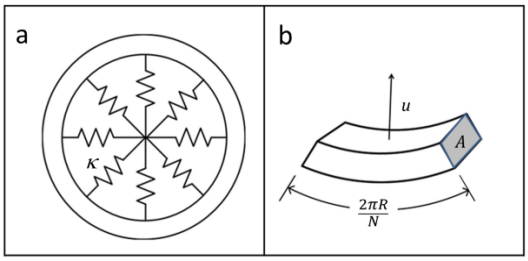

Figure 1. Schematics of (a) flexible ring with radial stiffness and (b) single tire segment

$$[\boldsymbol{K}]\{\boldsymbol{u}\} = \{\boldsymbol{F}\} \tag{1}$$

Note that this derivation includes relatively large deformations, approaching, but not including, the point of rim strike (when the tire sidewall is folded such that the upper portion is in direct contact with the lower portion and there is a discontinuous and dramatic increase in apparent stiffness). That is, the radial stiffness of each segment is assumed to be linear. Next the stiffness matrix $[\boldsymbol{K}]$ is developed, followed by a reduced order parameterization of the matrix using one stiffness and two shape parameters.

Derivation of the Stiffness Matrix

The quasi-static equation resulting from the application of Hamilton's principle for the distribution of energy and work throughout the tire is written as Equation (2).

$$\int_{t_1}^{t_2} (\delta U_b - \delta U_s - \delta U_r + \delta U_w) dt = 0 \qquad \forall t_1, t_2 \tag{2}$$

The virtual changes are computed as Equations (3) - (6), where spatial derivatives are represented by the commonly used prime notation (e.g., first spatial derivative of radial displacement is u')

$$\delta U_b = EIu''''\delta u \tag{3}$$

$$\delta U_s = GAu''\delta u \tag{4}$$

$$\delta U_r = \kappa u \delta u \tag{5}$$

$$\delta U_w = f\delta u \tag{6}$$

Continuity is enforced through the boundary conditions on the radial deformations and their spatial derivatives as given in Equation (7).

$$u|_x = u|_{x+2\pi R},\ u'|_x = u'|_{x+2\pi R},\ u''|_x = u''|_{x+2\pi R},\ u'''|_x = u'''|_{x+2\pi R} \tag{7}$$

The stiffness equation for each segment is then simplified to Equation (8).

$$EIu'''' + GAu'' + \kappa u = f \tag{8}$$

To reduce the required notation, the six physical properties (E, I, G, A, κ, and R) are grouped into three tire stiffness parameters (γ_b, γ_s and γ_r) as defined in Table 1. The tire stiffness parameters are invariant for a specific tire and positive valued for all tires. Most notably the tire stiffness parameters are not a function of the discretization process.

Table 1. Tire stiffness parameters and discretized radial force

$\gamma_b = EI(2\pi R)^{-3}$	Distributed bending stiffness
$\gamma_s = GA(2\pi R)^{-1}$	Distributed shear stiffness
$\gamma_r = \kappa(2\pi R)$	Distributed radial stiffness
$F_n = \frac{f}{N}(2\pi R)$	Radial force on n^{th} tire segment

The stiffness equation for each segment is then rewritten as Equation (9).

$$\gamma_b(2\pi R)^3 u'''' + \gamma_s(2\pi R)u'' + \gamma_r(2\pi R)^{-1}u = f \tag{9}$$

Defining Stiffness and Shape Parameters

Next the model is discretized into N equal segments via a finite difference method. The fourth spatial derivative of the radial displacement for the n^{th} tire segment is approximated by Equation (10); the second spatial derivative is found in a similar manner.

$$u_n'''' \simeq \frac{u_{n-2} - 4u_{n-1} + 6u_n - 4u_{n+1} + u_{n+2}}{\left(\frac{2\pi R}{N}\right)^4} \tag{10}$$

A second set of parameters is introduced to simplify the subsequent analysis, beginning with discretizing the continuous stiffness equation given in Equation (9). The discrete stiffness equation for the n^{th} tire segment is expressed as Equation (11), where the radial force on the n^{th} tire segment, F_n, is defined in Table 1.

$$k_0\alpha_2 u_{n-2} + k_0\alpha_1 u_{n-1} + k_0 u_n + k_0\alpha_1 u_{n+1} + k_0\alpha_2 u_{n+2} = F_n \tag{11}$$

The model stiffness (k_0) and shape parameters (α_1 and α_2) are defined in terms of the tire stiffness parameters of Table 1. For convenience, the conversion between sets of parameters is defined by a pair of transformation matrices given in Equation (12) and Equation (13).

$$\begin{bmatrix}\gamma_1\\ \gamma_2\\ \gamma_3\end{bmatrix} = \begin{bmatrix}0 & 0 & \frac{1}{N^3}\\ 0 & \frac{1}{N} & \frac{4}{N}\\ N & 2N & 2N\end{bmatrix}\begin{bmatrix}k_0\\ k_0\alpha_1\\ k_0\alpha_2\end{bmatrix} \tag{12}$$

$$\begin{bmatrix}k_0\\ k_0\alpha_1\\ k_0\alpha_2\end{bmatrix} = \begin{bmatrix}6N^3 & -2N & \frac{1}{N}\\ -4N^3 & N & 0\\ N^3 & 0 & 0\end{bmatrix}\begin{bmatrix}\gamma_1\\ \gamma_2\\ \gamma_3\end{bmatrix} \tag{13}$$

The usefulness of the tire stiffness parameters, $\{\gamma\}$, is that they are convenient to describe the distributed stiffness equation, Equation (9), and they are not affected by the number of tire segments chosen to discretize the system. The model stiffness and shape parameters (k_0, α_1, α_2), by contrast, are convenient for the discretized stiffness equation, Equation (11), with which the reminder of this work is concerned. Consider a typical modeling exercise in which the number of segments is to be increased. Once the model stiffness and shape parameters are identified for a model with the original number of segments, the corresponding invariant tire stiffness parameters, $\{\gamma\}$, can be calculated using Equation (12). If a new number of segments is desired, the corresponding values for the new model stiffness and shape parameters is calculated using Equation (13) and the invariant tire stiffness parameters.

Parameterized Stiffness Matrix

The symmetry of a physical tire, enforced by Equation (7), results in a circulant Toeplitz stiffness matrix $[\boldsymbol{K}]$, as shown in Equation (14), that comprises two parts: the single parameter k_0 defines the model stiffness and the model shape

matrix $[\boldsymbol{\alpha}]$ (defined by the two model shape parameters α_1 and α_2) that defines the relative deformations of the tire when acted upon by geometric constraints.

$$[\boldsymbol{K}] = k_0 \begin{bmatrix} 1 & \alpha_1 & \alpha_2 & 0 & \cdots & \alpha_2 & \alpha_1 \\ \alpha_1 & 1 & \alpha_1 & \alpha_2 & \cdots & 0 & \alpha_2 \\ \alpha_2 & \alpha_1 & 1 & \alpha_1 & \vdots & 0 & 0 \\ 0 & \alpha_2 & \alpha_1 & 1 & \cdots & 0 & 0 \\ \vdots & \vdots & \vdots & \vdots & \vdots & \vdots & \vdots \\ \alpha_1 & \alpha_2 & 0 & 0 & \cdots & \alpha_1 & 1 \end{bmatrix} = k_0[\boldsymbol{\alpha}] \tag{14}$$

DEVELOPMENT OF CONSTRAINT MODES

The Guyan static reduction method [17] is used to reduce the order of the stiffness matrix in Equations (15)-(18) by imposing geometric boundary constraints on the active degrees of freedom. The degrees of freedom, defined as the radial deformations of the tire $\{\boldsymbol{u}\}$, are categorized into active and omitted sets, represented by superscripts '*a*' and '*o*' respectively. In general, the geometric boundary constraints must be a subset of the active degrees of freedom. In the tire modeling case with which this work is concerned, the active constraints are exclusively comprised of those degrees of freedom in contact with the road surface. The degrees of freedom are reordered and written as vector $\{\widehat{\boldsymbol{u}}\}$ such that the active degrees of freedom occupy the first positions in the vector, followed by the omitted degrees of freedom, via an orthogonal sorting matrix, *S*, as shown in Equation (15).

$$\{\boldsymbol{u}\} = [[\boldsymbol{S}^a] \quad [\boldsymbol{S}^o]] \begin{Bmatrix} \{\widehat{\boldsymbol{u}}^a\} \\ \{\widehat{\boldsymbol{u}}^o\} \end{Bmatrix} = [\boldsymbol{S}]\{\widehat{\boldsymbol{u}}\}, \quad \{\widehat{\boldsymbol{u}}\} = [\boldsymbol{S}]^T\{\boldsymbol{u}\} \tag{15}$$

The stiffness matrix and the force vector must be similarly reordered as given in Equation (16).

$$\left[\widehat{\boldsymbol{K}}\right] = [\boldsymbol{S}]^T[\boldsymbol{K}][\boldsymbol{S}], \quad \left\{\widehat{\boldsymbol{F}}\right\} = [\boldsymbol{S}]^T\{\boldsymbol{F}\} \tag{16}$$

The reordered stiffness equation is then partitioned according to the active and omitted degrees of freedom as given in Equation (17).

$$\left[\widehat{\boldsymbol{K}}\right]\{\widehat{\boldsymbol{u}}\} = \begin{bmatrix} [\widehat{\boldsymbol{K}}^{aa}] & [\widehat{\boldsymbol{K}}^{ao}] \\ [\widehat{\boldsymbol{K}}^{oa}] & [\widehat{\boldsymbol{K}}^{oo}] \end{bmatrix} \begin{Bmatrix} \{\widehat{\boldsymbol{u}}^a\} \\ \{\widehat{\boldsymbol{u}}^o\} \end{Bmatrix} = \begin{Bmatrix} \{\widehat{\boldsymbol{F}}^a\} \\ \{\boldsymbol{0}\} \end{Bmatrix} = \left\{\widehat{\boldsymbol{F}}\right\} \tag{17}$$

Given a set of active constraints, $\{\widehat{\boldsymbol{u}}^a\}$, the omitted constraint vector $\{\widehat{\boldsymbol{u}}^o\}$ is written as Equation (18). The constraint mode for this particular set of active constraints is written as Equation (20).

$$\{\widehat{\boldsymbol{u}}^o\} = -\left[\widehat{\boldsymbol{K}}^{oo}\right]^{-1}\left[\widehat{\boldsymbol{K}}^{oa}\right]\{\widehat{\boldsymbol{u}}^a\} \tag{18}$$

In this work, the stiffness matrix is defined in terms of an overall stiffness parameter and two shape parameters, as developed in Equation (14). The reordered stiffness submatrices are then given by Equation (19) as

$$\left[\widehat{\boldsymbol{K}}^{oo}\right] = [\boldsymbol{S}^o]^T\,(k_0[\boldsymbol{\alpha}])[\boldsymbol{S}^o] \text{ and } \left[\widehat{\boldsymbol{K}}^{oa}\right] = [\boldsymbol{S}^o]^T\,(k_0[\boldsymbol{\alpha}])[\boldsymbol{S}^a] \tag{19}$$

The omitted constraint vector becomes solely dependent on the shape parameters and the active constraint vector, as developed in Equation (20).

$$\{\widehat{\boldsymbol{u}}^o\} = -([\boldsymbol{S}^o]^T[\boldsymbol{\alpha}][\boldsymbol{S}^o])^{-1}([\boldsymbol{S}^o]^T[\boldsymbol{\alpha}][\boldsymbol{S}^a])\{\widehat{\boldsymbol{u}}^a\} \tag{20}$$

Finally, the complete displacement vector is written as a function of the active constraint vector in Equation (21).

$$\{\boldsymbol{u}\} = \left[[\boldsymbol{S}^a] - [\boldsymbol{S}^o]([\boldsymbol{S}^o]^T[\boldsymbol{\alpha}][\boldsymbol{S}^o])^{-1}([\boldsymbol{S}^o]^T[\boldsymbol{\alpha}][\boldsymbol{S}^a])\right]\{\widehat{\boldsymbol{u}}^a\} \tag{21}$$

Note that this mode shape is completely independent of the overall tire stiffness and the forces acting on the tire. Rather, the shape is purely a function of the geometric boundary conditions (captured by the active constraint vector, $\{\widehat{\boldsymbol{u}}^a\}$, and the corresponding orthogonal sorting matrix, $[\boldsymbol{S}]$) and the two shape parameters α_1 and α_2. The issue then, is to deduce the active constraints.

Deducing Active Constraints

Whether a new active constraint must be added and, if so, which active constraint must be added is based on the impingement of the road surface on the tire surface. It is tempting to simply compare the relative positions of the undeformed shape of the tire and the road surface and sort the points by the magnitude of impingement. However, one point along the road surface may impinge farther into the undeformed tire's periphery than another, yet the former point may not be an active constraint while the later point is. This is demonstrated by the example in Figure 2. The undeformed tire (shown as a dashed line in Figure 2a) is impinged upon by three distinct points along the road surface (shown as a solid line). The points are labeled in Figure 2b according to their magnitude of impingement, from most to least, as A, B, and C. Although the impingement by point B is greater than that of point C, it should not be identified as an active constraint lest the unidirectional boundary condition be violated and the road is presumed to "pull" the tire down. In this way the process cannot be based on a Lagrangian formulation, since that assumes some *a priori* knowledge of which degrees of freedom are active, and thus motivates the development of a recursive process for adding active constraints.

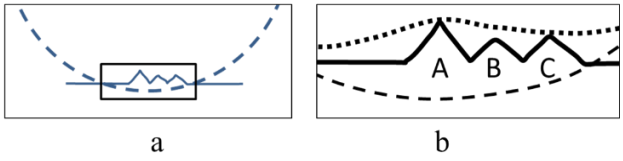

Figure 2. Deducing Active Constraints

Although the recursive process to identify the active constraints at the tire-road interface developed in this study is applicable to a wide range of tire models, including FE models and ring models, it is described herein for the tire model defined by Equation (20), and shown schematically in Figure 1. The first trial constraint mode is the undeformed shape of the tire (a circle, partly shown as a dashed line in Figure 3a), located at a prescribed vertical position above the road surface. The recursive process continues through steps a through e as follows:

a. Identify the set of degrees of freedom where the road surface impinges on the *current* trial constraint mode.
b. Sort the degrees of freedom with respect to the magnitude of impingement.
c. End the iteration process if no significant impingement exists.
d. Augment the current set of active degrees of freedom with the degree of freedom that has the greatest impingement (and those that impinge within some very small tolerance of that greatest impingement, if applicable).
e. Develop a new trial constraint mode based on this augmented set of active constraints.

For clarity, the set of active constraints at the tire-road interface is developed through a typical example. Consider a tire on a flat plate as shown in Figure 3 where the road, undeformed shape of the tire, and the deformed shape (the trial constraint mode) are shown as a solid, dashed, and dotted line respectively. The undeformed tire is the first trial constraint mode, shown in Figure 3a. The tire segment with the largest impingement is directly below the tire center and becomes the first active degree of freedom. Figure 3b shows the second trial constraint mode and the first active degree of freedom is shown as a single small circle. Figure 3c shows that two degrees of freedom have the same impingement (due to symmetry) and both are added to the set of active constraints and a new trial constraint mode is calculated. This process ends with Figure 3d when no significant impingement remains.

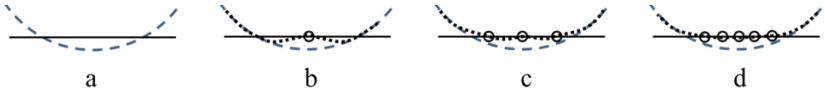

Figure 3. Recursive process to identify active constraints

Nonlinearity from Unidirectional Geometric Boundary Condition

It is clear that the stiffness equation, developed as Equation (8) for the continuous case and Equation (11) for the discrete case, are linear and time invariant as are the physical properties shown in Table 1. However real tires exhibit a nonlinear vertical force-deflection behavior that must be captured. The unidirectional geometric boundary conditions provide the mechanism by which this non-linear stiffness relationship is manifest. As the tire deflection

increases, more tire segments come into contact with the road surface and become active constraints as shown in Figure 4. As the tire first touches the road surface, only two segments are active and produce forces, shown as arrows in Figure 4a. As the deflection increases, the magnitude of the forces at the existing active constraints increases and additional degrees of freedom become active, as shown by the four arrows in Figure 4b. This addition of new constraints and the increase force magnitude continues with increased deflection (shown in Figure 4c).

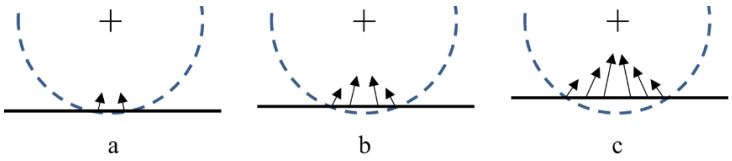

Figure 4. Additional radial forces added as deflection increases

EXPERIMENTAL VALIDATION

The experimental data used to validate this work is provided by Professor Schalk Els of the University of Pretoria, South Africa. The tire used is a Continental Conti-Trac AT 238/85 R16. Two quasi-static tests (a flat plate test and a cleat test) are performed that produce a resultant spindle force, F, with respect to the tire deflection, e, as shown in Figure 5a for the flat plate test and Figure 5b for the cleat test. The side length of the square cleat is 19 mm. In both cases an obstruction (plate or cleat) is gradually pressed toward the center of a tire that is rigidly fixed at the spindle. The model stiffness, k_0, and model shape parameters, α_1 and α_2, are identified using these two quasi-static tests. The flat plate test results are compared to the results from Ragheb, El-Gindy, and Kishawy [7]. The results of these two tests are shown in Figure 6 and Figure 7; in both figures the experimental results are shown as a solid line while the simulation results are shown as a dashed line.

a. Flat Plate b. Cleat

Figure 5. Schematics for Test Procedures

Validation via Flat Plate Testing

It is clear from Figure 6 that the nonlinear stiffening characteristic of the tire is captured by the constraint mode tire model via the unidirectional geometric boundary condition (see also Figure 4). The model parameters were optimized to minimize the maximum error, in this case 4%, throughout a reasonably large range of travel. For comparison purposes, Ragheb, El-Gindy, and Kishawy [7] used Mooney-Rivlin material properties to create detailed FE models of the tread and sidewall for a tire similar to the Michelin Off-road 12.00R20 XML TL 149J (a somewhat larger tire than that used in the present study). The FE model produced quasi-static flat-plate test results that were within 10-15% of the experimental results (depending on tire pressure). Also of note is that the nonlinearity in their simulation was negligible whereas the current study produces results that are clearly, though not dramatically, nonlinear.

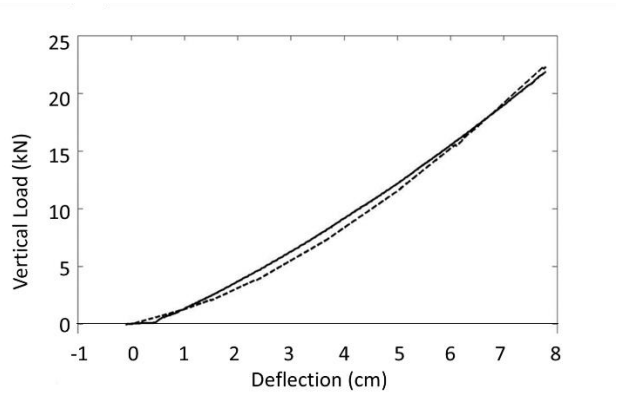

Figure 6: Flat-plate experimental and simulated force, F, with respect to the deflection, e

In this example, the shear and radial stiffnesses are orders of magnitude smaller than the bending stiffness. To simplify future comparisons to these results, the model shape and stiffness parameters and tire stiffness parameters provided in Table 2 may be used.

Table 2. Simplified tire stiffness parameters and modeling parameters

Modeling Parameters (N=72)	**Tire Stiffness Parameters**
$\boldsymbol{k_0 = 7.053 \times 10^6}$	$\gamma_1 = 3.15$
$\boldsymbol{\alpha_1 = -2/3}$	$\gamma_2 = 0$
$\boldsymbol{\alpha_2 = 1/6}$	$\gamma_3 = 0$

Validation via Cleat Testing

The cleat test simulation results shown in Figure 7 show very good agreement throughout the range of deflection; the maximum error is 7%. The nonlinear stiffness property, in the form of a discontinuity, is clearly captured in this modeling technique. The discontinuity in stiffness occurs when the experimental deflection exceeds approximately 5cm, dividing the results into two regions. In the lower region the tire is suspended by the cleat and the contact area is constrained to the cleat surface only. In this lower region the stiffness is quite linear in both the experimental results and the simulated results. This is expected because there are no additional unidirectional boundary constraints added as the deflection increases in this lower region. There is a dramatic change in the stiffness as deflection increases to the point where the tire tread touches the surface below the cleat as shown in the lower inset picture in Figure 7. Note that this discontinuity in stiffness is captured by the constraint mode tire model even though a simple linear model is used to predict the radial deflection of the tire surface.

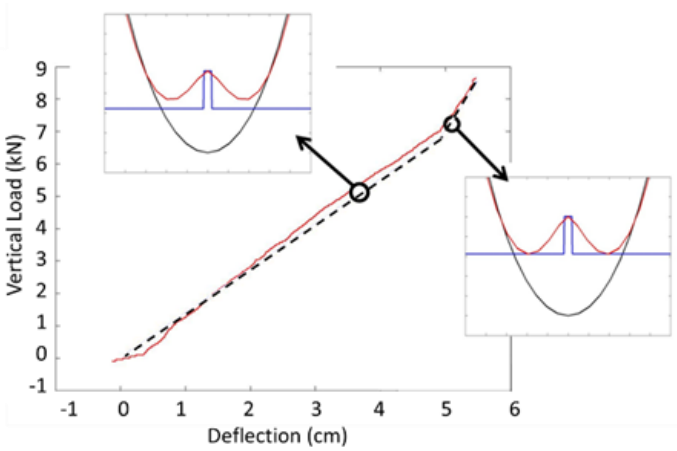

Figure 7: Cleat experimental and simulated force, F, with respect to the deflection, e

DISCUSSION

It is envisioned that the constraint mode tire model developed in this work can serve as a morphological filter. That is, this constraint mode tire model can be used to pre-filter the surface once, providing the required bridging and enveloping properties of the tire. A simpler tire model (perhaps a simple linear point-follower) could be used in the iterative design process to provide fast yet reliable spindle force predictions for vehicle dynamic simulation and reliability evaluation. Specifically, an effective road profile could be estimated given an actual profile by simulating the constraint mode tire model traveling over an actual profile given a constant spindle load. It is hoped that a small sacrifice in accuracy will result in an order of magnitude increase in computational speed. Preliminary results shown in Figure 8 where the actual profile is shown as a solid grey line and the effective road profile is shown as a dashed black line. In this example both the bridging and enveoloping proerties are evident (including the bridging of deep narrow cracks) which is encouraging for further study.

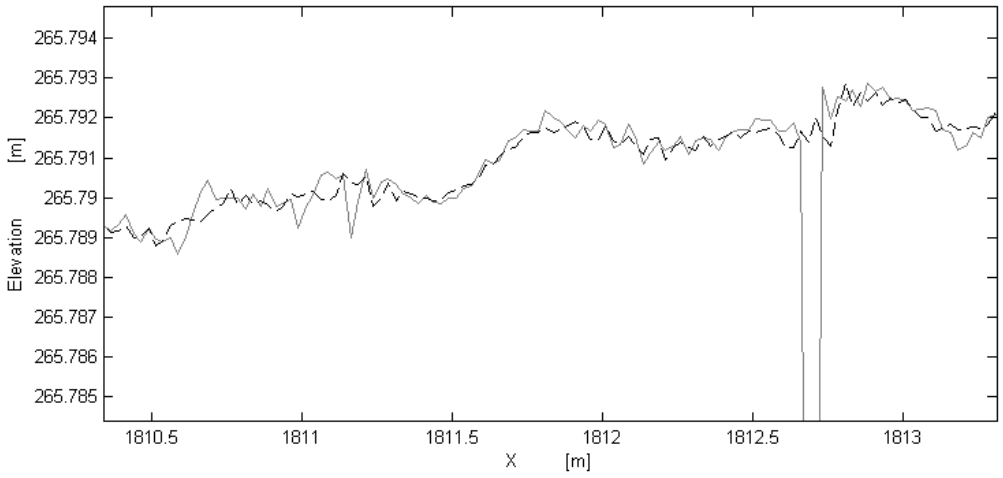

Figure 8: Potential use as Morphological Pre-Filter

CONCLUSIONS

The main contribution of this work is the development of a computationally efficient, linear, planar, quasi-static tire model that accurately predicts a tire's lower-frequency, reasonably large amplitude, nonlinear stiffness relationship.

One major development is that the model is parameterized by a single stiffness parameter and two shape parameters. The implication of this development is that the tire's deformed shape is completely independent of the overall tire stiffness and the forces acting on the tire. Rather, the shape is purely a function of the geometric boundary conditions and the two shape parameters α_1 and α_2. This simple model produces nonlinear stiffness when simulating a flat plate test and a discontinuous stiffness when simulating a cleat test, in both cases producing reasonable force predictions. The nonlinear behavior stems from the unidirectional geometric boundary conditions that are preserved during the recursive method developed to deduce the active constraints. A simple example demonstrates that simpler algorithms that do not use this new recursive method can erroneously define non-active constraints to be active. This may produce the effect of the road surface "pulling" the tire down. This model strikes a balance between heuristic tire models (such as a linear point-follower) that lack the fidelity to make accurate chassis load predictions and computationally intensive models that cannot provide timely predictions. It is hoped that this tire model is used as an integral part of computationally efficient and accurate vehicle dynamic simulations that are critical throughout the iterative design process.

ACKNOWLEDGEMENTS

The Automotive Research Center (ARC), a U.S. Army center of excellence in modeling and simulation of ground vehicles, is gratefully acknowledged for their support of this research. The authors wish to thank Professor Schalk Els of the University of Pretoria for providing the experimental data used throughout this work.

REFERENCES

[1] Willumeit, H.-P, and Boehm F., 1995, "Wheel Vibrations and Transient Tire Forces", Vehicle System Dynamics, 24, pp.525-50.

[2] Umsrithong, A., Stochastic Semi-Empirical Transient Tire Models, in Mechanical Engineering. 2012, Virginia Tech: Blacksburg, VA

[3] Mousseau, C. W., and Hulbert, G. M., 1996, ""The Dynamics responses of Spindle Forces Produced by a Tire Impacting Large Obstacles in a Plane", J. Sound and Vibration, 195(5), pp. 775-96.

[4] Darnell, I., Hulbert, G. M., and Mousseau C. W., 1997, "An Efficient Three-Dimensional Tire Model", Mech, Struct. & Mach., 25(1), pp. 1-19.

[5] Hanley, R., Crolla, D., and Hauke, M., 2001, "Tire Modeling for Misuse Situations", SAE Paper No. 2001-01-0748.

[6] Burke, A. M., and Olatunbosun, O. A., 1997, "Contact Modeling of the tyre/Road Interface", Int. J. of Vehicle Design, 18(2), pp. 194-202.

[7] Ragheb, H., El-Gindy, M., and Kishawy, H., "Development of a Combat Vehicle FEA Tire Model for Off-Road Applications," SAE Technical Paper 2013-01-0632, 2013, doi:10.4271/2013-01-0632.

[8] Van Oosten, J. J. M., and Jansen, S. T. H., 1999, "High Frequency Tire Modeling Using SWIFT-Tyre", Int'l ADAMS Users' Conference, Berlin, Germany.

[9] Zegelaar, P.W.A.P., H. B., The In-plane Dynamics of Tyres on Uneven Roads. Vehicle System Dynamics, 1996: p. 714-730

[10] Loo, M., A Model Analysis of Tire Behavior under Vertical Loading and Straight-Line Free Rolling. Tire Science and Technology, 1985. 13(2): p. 67-90.

[11] Badalamenti, J.M.D., G. R., Radial-Interradial Spring Tire Models, Acoustic, Stress and Reliability in Design. Journal of Vibration, 1988. 110(1): p. 70-75.

[12] Gillespie, T.D., Fundamentals of Vehicle Dynamics. 1992, Warrendale, PA: Society of Automotive Engineers, Inc.

[13] Takayama, M.Y., K., Simulation Model of Tire Vibration. Tire Science and Technology, 1984. 11(1): p. 38 – 49.

[14] Ferris, J.B., Capturing Planer Tire Enveloping Properties Using Static Constraint Modes, in ASME 2006 International Mechanical Engineering Congress and Exposition (IMECE2006), Dynamic Systems and Control Division 2006: Chicago, Illinois, USA p. IMECE2006-15260 pp. 467-472.

[15] Hurty, W.C., Dynamic Analysis of Structural Systems Using Component Modes. AIAA Journal, 1965. 3(4): p. 678-685,

[16] Gladwell, G.M.L., Banch Mode Analysis of Vibrating Systems. Journal of Sound and Vibration, 1964. 1(1): p. 41-59,

[17] Guyan, R.J., Reduction of Stiffness and Mass Matrices. AIAA Jounrnal, 1965. 3(2): p. 380.

[18] Ma, R., A.A. Reid, and J.B. Ferris. Capturing Planar Tire Properties Using Static Constraint Modes, ASME-DSCC. 2012. Ft. Lauderdale, FL.